JCTC Journal of Chemical Theory and Computation

Parametrization and Validation of Intramolecular Force Fields Derived from DFT Calculations

Ivo Cacelli* and Giacomo Prampolini

Dipartimento di Chimica e Chimica Industriale, Universita di Pisa, via Risorgimento 35, I-56126 Pisa, Italy

Received May 15, 2007

Abstract: The energy and its first and second geometrical derivatives obtained by DFT calculations for a number of conformations of a single molecule are used to parametrize intramolecular force fields, suitable for computer simulations. A systematic procedure is proposed to adequately treat either fully atomistic or more simplified force fields, as within the united atom approach or other coarse grained models. The proposed method is tested and validated by performing molecular dynamics simulations on several different molecules, comparing the results with literature force fields and relevant experimental data. Particular emphasis is given to the united atom approach for flexible molecules characterized by "soft" torsional potentials which are known to retain a high degree of chemical specificity.

1. Introduction

Thanks to the massive increase of computational resources of the past two decades, the study and design of novel materials possessing the desired physical, chemical, and biological requirements can be significantly aided by a detailed investigation on structure and interactions at molecular scale. In this theoretical approach to material science, computer simulations methods[1,2] such as Monte Carlo (MC) and Molecular Dynamics (MD) have been employed successfully in many complex systems as, for instance, clays,[3] nanocomposites,[4] polymers,[5−7] liquid crystals,[8] macromolecules,[9] or biological membranes.[10] In MC or MD simulations, all the information on the molecular framework and interactions are encrypted in the adopted force field (FF), which can be considered as the link between the microscopic description and the resulting structural and dynamic macroscopic properties.

In computer simulation studies of advanced materials two main problems arise, due to the complexity of the intra- and intermolecular forces. First, notwithstanding the usually large dimensions of the forming molecules, small differences in the specific molecular structure may produce impressive variations in the resulting material properties due to the delicate interplay between energetic and entropic effects. This implies that caution must be used in extending the straightforward adoption of the most widely employed FFs[11−17] to target molecules. Second, the wide range of length and time scales that characterizes the dynamics of complex systems impose some limitations on the complexity of the FF that can be adopted. Consequently, increasing attention has been devoted to the construction of united atom (UA) or coarse grained (CG) models,[6,10,18−20] capable of capturing the main physics of the problem while reducing the computational expense with respect to fully atomistic (FA) descriptions. These two issues (transferability problems and computational advantages of simplified FFs) convinced us to work toward a route that could allow the parametrization of FFs specifically suited for a definite target molecule rather than performing ad hoc empirical corrections on potential parameters transferred from the general literature FFs.

To make up for the lack of specificity in the standard FF description of the molecular interactions, our group has recently proposed the Fragmentation Reconstruction Method (FRM),[21,22] for the calculation of the intermolecular potential energy surface (PES) of large molecules from ab initio data only. Once the two-body potential has been computed for a number of dimer arrangements, the parametrization of an intermolecular FF of the desired complexity can be performed by a least-square fitting. The obtained parameters, employed in simulations, can then be validated through the

* Corresponding author e-mail: ivo@dcci.unipi.it.

10.1021/ct700113h CCC: $37.00
Published on Web 08/21/2007

comparison of the resulting macroscopic properties with the relevant experimental measures. Up to now, the whole approach has been successfully tested in the field of liquid crystals for both UA[23−26] and CG[27] models of some mesogenic molecules.

With regards to the intramolecular part of the potential, a great variety of internal FFs has been proposed in the last two decades,[11,12,14,17,28−30] and many different sets of parameters can be found in the literature. Among these, it may be useful to distinguish between class I and class II FFs (see e.g. ref 29), on the basis of the complexity of their analytical expressions: class I FFs[11,14,17] are diagonal in a given set of internal coordinates and only contain harmonic terms for bond stretching and angle bending, while the more recent class II FFs[12,28,29] usually include anharmonic terms and off-diagonal couplings. Broadly speaking, while the former are designed for simulations of large systems in condensed phase, the latter have been mostly used for the study of structures and energetics in the gas phase.[31]

The attempt to extend literature intramolecular parameters to a well-defined target molecule requires a distinction between "hard" and "soft" internal degrees of freedom. The formers, such as bond stretching and bond angle bending, are usually less affected by the molecular environment, and the transferability of literature FFs is expected to be satisfactory for most purposes. Nonetheless, many cases have been reported where the intramolecular description achieved by standard class I FFs was found not to be adequate as, for instance, the reproduction of spectroscopic properties[32,33] or in the presence of nonstandard structures as heteroaromatic rings.[34] The situation is even more complex for flexible molecules, where flat energy profiles and small energy barriers are found for "soft" internal degrees of freedom, generally dihedral angles. This causes different conformations to be populated even at low temperatures with a marked sensitivity to both intra- and intermolecular environment. An accurate description of these torsional curves is therefore necessary, and a reparametrization of some specific torsions has often been performed[20,24,35−38] to correct the standard literature FFs. More importantly, when dealing with large molecules, the necessity of adopting novel UA or CG models calls for new parametrizations of those intramolecular potentials which describe the forces between the nonatomistic sites.[27,39] To our knowledge, no attempt has yet been made to propose a systematic approach capable of providing a set of intramolecular parameters for newly designed CG models.

In this context, the method here proposed is intended to provide a complete parametrization of intramolecular FFs of a target molecule, at various degrees of complexity, on the basis of quantum mechanical (QM) calculations only. For these reasons the computed FF will be labeled QMD, i.e., quantum mechanics derived. The implementation of this method should provide both spectroscopic quality FFs or less complex intramolecular parametrizations suitable for simulations of condensed phases.

Similar QM-derived approaches have already been proposed by other groups[28,30,40] who employed QM ab initio data to parametrize intramolecular FFs at several levels of complexity. However, these studies aim at providing spectroscopic quality class II FFs, and none of these considers intramolecular parametrizations in the UA approach. It should be pointed out that, owing to the fictitious molecule inherent to the UA approach, a UA-FF cannot be rigorously derived from QM data. Nevertheless, as discussed in this paper, suitable approximations can still be made in order to judiciously use the QM information in UA-FF parametrization. Once the model to be adopted for the target molecule has been chosen, the present method should thus provide the best values of the parameters entering the assigned functions of internal coordinates. In fact, as previously stressed, another peculiarity of the proposed approach with respect to other similar methods as, for example, QMFF[29] is to privilege FF specificity rather than FF transferability. In addition to the above-mentioned reasons, this strategy is also advisable for the increase of computational resources, which allow nowadays to perform accurate QM calculations even for large systems, as for instance liquid crystal forming molecules,[23,24,38] thus both providing a QM database to calibrate specific intramolecular FFs and reducing the need of invoking transferability. A different situation is encountered when treating very large biological systems, where the dimension of the involved molecules rules out QM calculations, and transferable parameters are strongly needed to perform computer simulation studies.

The paper is organized as follows: in section 2 the theory of the method is described, and the computational details of the employed techniques are given in section 3. The first part of section 4 is devoted to the validation of the method for "hard" internal coordinates (IC). The intramolecular FFs, computed for several stiff heteroaromatic molecules, are employed in MD-FA simulations, and some of the resulting thermodynamic and structure properties are compared with both theoretical and experimental data. In the second part of section 4, the capability of the proposed approach to yield intramolecular FF for large, flexible molecules in the UA approach is tested. Finally, main conclusions are drawn in section 5.

2. Theory

The QMD-FF is modeled on the basis of QM results, namely energies, energy gradient, and Hessian matrix, for a number of molecular geometries. To make the formulas easier to be understood, the following notation will be adopted for the summation indices and symbols: i and j are used for the Cartesian coordinates (CCs) x or mass weighted Cartesian coordinates ($1 \div 3N$), μ and ν indicate the redundant internal coordinates[41,42] (RICs) q ($1 \div N_{\mathrm{RIC}}$), K and L run over the normal coordinates (NCs) Q ($1 \div 3N - 6$) ($3N - 5$ for linear molecules), g runs over the considered molecular geometries ($0 \div N_g$), a and b indicate the functions f used to represent the empirical FF and/or the number of linear parameters of the FF ($1 \div N_{\mathrm{func}}$), and s and t run over the quantities to be represented by the FF (energies, energy gradients and Hessian) for the considered geometries ($1 \div N_{\mathrm{points}}$).

The QMD-FF, to be used in molecular dynamics or molecular mechanics, is expressed through a linear combination of functions f_a of a set of RICs

$$V(q) = \sum_{a=1}^{N_{\text{func}}} p_a f_a(q) \tag{1}$$

where the q symbol collects all RICs. The functions may conveniently be expressed in terms of displacements with respect to a given reference geometrical conformation identified by the vector q^0

$$\Delta q_\mu = q_\mu - q_\mu{}^0 \tag{2}$$

Usually the RICs consist of all bond stretches, angle bendings, and dihedral torsions that can be obtained from a given connectivity criteria referred to the reference conformation. The inversion coordinate[43] can be included for atoms bonded to three other atoms. Nonbonded intramolecular interactions can also be added in order to make the FF more accurate. In usual FFs the number of RICs exceeds $3N-6$, and therefore they form a redundant set of coordinates. Although eq 1 has been written in a general form, each function f_a only depends on one or two RICs, as reported in detail later on (eqs 36−41).

2.1. Internal Coordinates Transformations. Since the Hessian and gradients are computed in CCs, whereas the FF is usually expressed through RICs, some coordinate transformation is required. For infinitesimal displacements with respect to a given geometrical conformation, the RICs are related to the nuclear CCs x through a noninvertible transformation

$$\delta q = B\delta x \tag{3}$$

where δq and δx are column vectors. The Wilson rectangular B matrix

$$B_{\mu i} = \left(\frac{\partial q_\mu}{\partial x_i}\right) \tag{4}$$

is related to the geometry the displacements are referred to and can be accurately computed both in analytical[44] and numerical ways.

The normal coordinates are computed from the Hessian matrix in CCs

$$H_{ij} = \left(\frac{\partial^2 E}{\partial x_i \partial x_j}\right) = E''_{ij} \tag{5}$$

obtained by a QM calculation at a given geometry. H is transformed to the mass weighted CCs form and diagonalized by a unitary matrix C

$$M^{-1/2} H M^{-1/2} C = C\Lambda \tag{6}$$

The matrix M is diagonal and for each CC contains the mass m of the related atom. The columns of the C matrix are the linear combinations of the mass weighted CCs that correspond to the NCs displacements

$$\delta Q_K = \sum_{i=1}^{3N} \sqrt{m_i} C_{iK} \delta x_i \tag{7}$$

or in matrix form

$$\delta Q = \tilde{C} M^{1/2} \delta x \tag{8}$$

where δQ and δx are column vectors. In the case the geometry corresponds to an absolute or local energy minimum, $3N - 6$ eigenvalues Λ_K are positive and refer to vibrations, whereas the 3 translational and 3 rotational modes are identified by zero eigenvalues. In other cases negative eigenvalues can occur, and these do not correspond to vibrational modes. If all the NCs are retained, the transformation of eq 7 is fully invertible

$$\delta x = M^{-1/2} C \delta Q \tag{9}$$

The relation between the RICs and the NCs can be easily obtained exploiting the completeness of the CCs basis set. Using eqs 3 and 9

$$\delta q = B M^{-1/2} C \delta Q = T \delta Q \tag{10}$$

where the T matrix is defined as

$$T_{\mu K} = \left(\frac{\partial q_\mu}{\partial Q_K}\right) \tag{11}$$

Thus the RICs may be expressed in terms of the NCs, and the inclusion or not of the rotational and translational modes is uninfluential since they leave the RICs unchanged.

2.2. The Optimal Parameters of the Force Field. The best parameters for the QMD-FF in order to represent the internal molecular motion are obtained by minimizing the following merit function, written as a sum over the considered molecular geometries

$$I = \sum_{g=0}^{N_g} I_g \tag{12}$$

where

$$I_g = W_g[(E_g - E_0) - V_g]^2 + \sum_{K=1}^{3N-6} \frac{W'_{Kg}}{3N-6}[E'_{Kg} - V'_{Kg}]^2 + \sum_{K \le L}^{3N-6} \frac{2W''_{KLg}}{(3N-6)(3N-5)}[E''_{KLg} - V''_{KLg}]^2 \tag{13}$$

The indices K and L (capital letters) run over the normal coordinates and include all the modes except for the rotational and translational ones. E_g is the total energy obtained by a QM calculation, and E_0 is the same at the reference geometry ($g = 0$). E'_{Kg} (E''_{KLg}) is the energy gradient (Hessian) at a given geometry with respect to the NC evaluated at the same geometry. V, V', and V'' are the corresponding quantities calculated by the FF in eq 1. The constants W, W', and W'' weight the several terms at each geometry and can be chosen in order to drive the results depending on the circumstances. The energy, gradient, and Hessian terms are normalized in order to account for the different number of terms and to make the weights independent from the number of atoms in the molecule.

To compute the energy derivatives entering the merit function (13) we have to perform some transformations since no derivative is originally expressed with respect to the NCs. Indeed standard quantum chemistry programs provide de-

rivatives E' and E'' with respect to CCs. Using the above relations and exploiting the completeness of the CCs, the transformation is simple

$$E'_K = \left(\frac{\partial E}{\partial Q_K}\right) = \sum_{i=1}^{3N}\left(\frac{\partial E}{\partial x_i}\right)\left(\frac{\partial x_i}{\partial Q_K}\right) = \sum_{i=1}^{3N} E'_i\, m_i^{-1/2}\, C_{iK} \quad (14)$$

or in matrix form

$$[E']_{\mathrm{NC}} = \tilde{C} M^{-1/2} [E']_{\mathrm{CC}} \quad (15)$$

where the square parentheses indicate column vectors of energy gradients computed with respect to the NCs and the CCs. The QMD-FF energy gradients at a given geometry

$$V'_K = \sum_{a=1}^{N_{\mathrm{func}}} p_a \left(\frac{\partial f_a}{\partial Q_K}\right) = \sum_{a=1}^{N_{\mathrm{func}}} p_a\, f'_{aK} \quad (16)$$

can be conveniently computed using the derivatives of the basis function with respect to the RICs, that is

$$\left(\frac{\partial f_a}{\partial Q_K}\right) = \sum_{\mu=1}^{N_{\mathrm{RIC}}}\left(\frac{\partial f_a}{\partial q_\mu}\right)\left(\frac{\partial q_\mu}{\partial Q_K}\right) = \sum_{\mu=1}^{N_{\mathrm{RIC}}}\sum_{i=1}^{3N}\left(\frac{\partial f_a}{\partial q_\mu}\right) T_{\mu K} \quad (17)$$

or in matrix form

$$[f'_a]_{\mathrm{NC}} = \tilde{T} [f'_a]_{\mathrm{RIC}} \quad (18)$$

The Hessian matrix of the QM calculation in NCs

$$E''_{KL} = \left(\frac{\partial^2 E}{\partial Q_K \partial Q_L}\right) \quad (19)$$

is obtained from the Hessian matrix in the CC basis according to

$$[E'']_{\mathrm{NC}} = \tilde{C} M^{-1/2} [E'']_{\mathrm{CC}} M^{-1/2} C \quad (20)$$

The second derivatives of the FF are a bit more complicated since they involve derivatives of the B matrix and are conveniently expressed in explicit form

$$\left(\frac{\partial^2 f_a}{\partial Q_K \partial Q_L}\right) = \sum_{\mu\nu=1}^{N_{\mathrm{RIC}}} T_{\mu K}\left(\frac{\partial^2 f_a}{\partial q_\mu \partial q_\nu}\right) T_{\nu L} + \sum_{\mu\nu=1}^{N_{\mathrm{RIC}}} T_{\mu K}\left(\frac{\partial f_a}{\partial q_\nu}\right)\left(\frac{\partial T_{\nu L}}{\partial q_\mu}\right) \quad (21)$$

As shown in eq 1, the QMD-FF is linear in the p parameters, thus the least-squares minimization of functional (13) can be written as

$$\sum_{a}^{N_{\mathrm{func}}}\sum_{s}^{N_{\mathrm{point}}} \alpha_{bs} W_s \alpha_{as} p_a = \sum_{s}^{N_{\mathrm{point}}} \alpha_{bs} W_s \beta_s \quad (22)$$

where the index s runs over the collections [g], [Kg], and [KLg] defined in eq 13 for energy, gradient, and Hessian, respectively. Following this notation the matrix α and the vector β are defined as

$$\alpha_{as} = f_{as} \text{ or } f'_{as} \text{ or } f''_{as}; \quad \beta_s = E_s \text{ or } E'_s \text{ or } E''_s$$

and

$$W_s = W_s \text{ or } \frac{W'_s}{3N-6} \text{ or } \frac{W''_s}{(3N-6)(3N-5)}$$

where f's are the functions of eq 1, E, E', and E'' are the functions of the QM data, and W, W', and W'' are the weights of the merit function (13). Thus, defining

$$A = \alpha W \tilde{\alpha}$$

$$b = \alpha W \beta$$

one has to solve a standard linear equation in the form

$$Ap = b \quad (23)$$

where A is a symmetric matrix.

In usual FF it is convenient for practical purposes to employ functions of the RIC that will be in general redundant over the considered points. The scalar product between the FF functions is defined as

$$f_a \cdot f_b = \sum_{s=1}^{N_{\mathrm{point}}} W_s\ f_{as}\ f_{bs} \quad (24)$$

and the redundancy strongly depends on the number and type of points included in the fitting. However in general the f set might not be linearly independent. This leads to a singular A matrix, and the direct inversion method cannot be used to solve the linear system (23). On the contrary, the Singular Value Decomposition method[40,45] adapted to symmetric matrices is adequate and provides a stable solution of the linear system.

2.3. United Atom Theory. In many molecular simulations a group of atoms whose individual behavior is considered not to be crucial for the properties to be investigated can be grouped in a single interaction site. This approach, henceforth named United Atom (UA), allows saving computational time and simultaneously removes some high-frequency vibrational modes which can limit the integration time step in MD simulations. The most common example concerns aliphatic chains where each CH_2 group is treated as a single interaction site (C_2) with FF parameters accounting for the effect of the hydrogen atoms both in the nonbonded interactions and electrostatic charge. Despite recent work that has been done for some torsional potentials,[20] usually the intramolecular FF parameters of "hard" IC are not changed in the UA approach, thus the parameters driving the C_2-C_2-C_2 stretching and bending motion in the aliphatic chains are the same as those commonly employed in the FA description.

In the UA approximation the involved atoms are considered to move as a single point with the consequence that the translational movements with respect to the rest of the molecule can be somehow taken into account, but the relative rotational movements are irreparably lost. In other words a three-dimensional object described by 6 coordinates is transformed into a single point described by 3 coordinates. Even in the (nonrealistic) hypothesis that there exists some local vibrational modes much faster than those involving the atoms close to the UA, this approximation affects the motion of the neighboring atoms. Thus the remaining vibrational frequencies are altered by the UA approach, and it is

convenient focusing on the representation of the intramolecular potential energy rather than on the vibrational analysis.

In this paper the UA atom approach, consistently with the previous FA approach, is treated on the basis of ab initio calculation of energies, gradients, and Hessian. The main problem is concerned with the transformation of the gradient vector and Hessian matrix in eq 13 in case the number of effective atoms is less than than the number of true atoms in the molecule. Let us consider for simplicity the case of a single UA in which N_{UA} atoms are grouped together. We use the indices μ and ν for the Cartesian coordinates referred to as the atoms involved in the UA and the indices a and b for those of the remaining atoms not involved in the UA (in this section we are forced to change the previous notation). For simplicity we suppose that only one atom in the UA group is linked to the unaltered atoms. The first-order energy expansion around a given geometry is

$$E^{(1)} = \sum_{a}\sum_{s}^{x,y,z} E'_{as}\delta t_{as} + \sum_{\mu}\sum_{s}^{x,y,z} E'_{\mu s}\,\delta t_{\mu s} \tag{25}$$

where t_{as} represents the sth component of the CC of the ath atom. The new gradient vector of the united atom U for a given geometry is transformed according to the simple expression

$$E'_{Us} = \sum_{\mu} E'_{\mu s} \quad (s = x,y,z) \tag{26}$$

where E'_{U} represents the energy gradient with respect to the UA displacements. This expression is consistent with the hypothesis that the UA represents a set of internally frozen atoms: $\delta t_{Us} = \delta t_{\mu s}$ ($\mu = 1...N_{UA}$) and holds for simultaneous translations but not for rotations of the grouped atoms.

The second-order energy is

$$E^{(2)} = \frac{1}{2}\sum_{ab}\sum_{sr}^{x,y,z} E''_{as,br}\delta t_{as}\delta t_{br} + \frac{1}{2}\sum_{\mu\nu}\sum_{sr}^{x,y,z} E''_{\mu s,\nu r}\delta t_{\mu s}\delta t_{\nu r} + \sum_{a\mu}\sum_{sr}^{x,y,z} E''_{as,\mu r}\delta t_{as}\delta t_{\nu r} \tag{27}$$

Defining the UA Hessian matrix as

$$E''_{Us,Ur} = \sum_{\mu\nu} E''_{\mu s,\nu r} \tag{28}$$

$$E''_{as,Ur} = \sum_{\mu} E''_{as,\mu r} \tag{29}$$

the energy expression becomes

$$E^{(2)} = \frac{1}{2}\sum_{ab}\sum_{sr} E''_{as,br}\delta t_{as}\delta t_{br} + \frac{1}{2}\sum_{sr} E''_{Us,Ur}\delta t_{Us}\delta t_{Ur} + \sum_{a}\sum_{sr} E''_{as,Ur}\delta t_{as}\delta t_{Ur}$$

$$= \frac{1}{2}\tilde{\delta}tE''\delta t \tag{30}$$

It is easy to verify that such a transformation of the Hessian matrix will preserve the three null eigenvalues due to translations, whereas the rotational modes of a molecule with UA included may lead to small (unphysical) energy contributions with the further undesirable consequence of small mixing between rotational and vibrational modes.

The two other quantities of the UA to be defined are the mass and the relative position. For the UAs considered in this paper (methylene and methyl groups) the mass was taken as the sum of the involved atoms. In the case where only one atom of the grouped atoms forms bonds with the rest of molecule, the natural choice for the position seems to make the UA coincident with that atom. However, other choices are possible; for example, the UA may be placed in the center of mass of the grouped atoms at the equilibrium geometry and/or its mass may be chosen in order to preserve the original inertia moments. Taking as criteria the magnitude of the rotational eigenvalues and the perturbation of the vibrational modes, these attempts do not lead to any improvement and were rejected. With the original choice the rotational eigenvalues at the equilibrium geometry are found to be much lower than the low-frequency vibrational modes, and the contamination is very small.

In summary the UA approach preserves some of the original atom−atom interactions contained in the Hessian matrix and leads to a useful simplification of the intramolecular energy hypersurface but does not allow conserving the rigorous implementation of the all-atom force field presented in this paper.

2.4. MD Model Force Field. The FF employed in MD simulations has the following expression: The intermolecular

$$E_{tot} = E_{inter} + E_{intra} \tag{31}$$

part, E_{inter}, is computed as

$$E_{inter} = E_{LJ} + E_{Coul} \tag{32}$$

where the long-range electrostatic term is

$$E_{Coul} = \sum_{i=1}^{N_{sites}}\sum_{j=1}^{N_{sites}} \frac{q_i q_j}{r_{ij}} \tag{33}$$

and a Lennard-Jones term has been employed for the short-range part, i.e.

$$E_{LJ} = \sum_{i=1}^{N_{sites}}\sum_{j=1}^{N_{sites}} 4\epsilon_{ij}\left[\left(\frac{\sigma_{ij}}{r_{ij}}\right)^{12} - \left(\frac{\sigma_{ij}}{r_{ij}}\right)^{6}\right] \tag{34}$$

where i and j belong to different molecules, and N_{sites} is the total number of interacting sites. The intermolecular parameters q_{ij}, σ_{ij}, and ϵ_{ij} were taken for all molecules from the OPLS[15,16] literature force field.

The intramolecular part of the QMD-FF is expressed as a sum of different terms, namely

$$E_{intra} = V(q) = E_{stretch} + E_{bend} + E_{Rtors} + E_{Ftors} + E_{Coupl} \tag{35}$$

The first three terms count for the "hard" IC, i.e., bond stretchings, angle bendings, and stiff angle dihedrals (Rdihedrals), as those that drive the planarity of aromatic rings and are expressed with harmonic potentials:

$$E_{\text{stretch}} = \frac{1}{2}\sum_{\mu}^{N_{\text{bonds}}} k_{\mu}^{s}(r_{\mu} - r_{\mu}^{0})^2 \quad (36)$$

$$E_{\text{bend}} = \frac{1}{2}\sum_{\mu}^{N_{\text{angles}}} k_{\mu}^{b}(\theta_{\mu} - \theta_{\mu}^{0})^2 \quad (37)$$

$$E_{\text{Rtors}} = \frac{1}{2}\sum_{\mu}^{N_{\text{Rdihedrals}}} k_{\mu}^{t}(\phi_{\mu} - \phi_{\mu}^{0})^2 \quad (38)$$

Conversely, the model functions employed for more flexible dihedrals (Fdihedrals) are the sums of periodic functions, namely

$$E_{\text{Ftors}} = \sum_{\mu}^{N_{\text{Fdihedrals}}} \sum_{j=1}^{N_{\cos_\mu}} k_{j\mu}^{d}[1 + \cos(n_j^{\mu}\phi_{\mu} - \gamma_j^{\mu})] \quad (39)$$

where $N_{\cos_\mu}$ is the number of cosine functions employed to describe the potential of the ϕ_μ dihedral. It is worth noticing that eqs 36−39 can be easily expressed in the formalism of eq 1 by setting $q_\mu = r_\mu$, θ_μ, and ϕ_μ, respectively. Following the notation introduced in eq 1, the last term of eq 35 can be written as

$$E_{\text{Coupl}} = \sum_{i}^{N_{\text{Coupl}}} V_i(q_\mu, q_\nu) \quad (40)$$

and may contain specific cross terms between the ICs q_μ and q_ν. The presence or absence of these off-diagonal coupling terms, which for instance may be of the form proposed in ref 29, discriminates between QMD-FFs of class II or class I. In this paper only couplings between soft dihedrals have been tested, which take the following expression

$$V_i(\phi_\mu, \phi_\nu) = \sum_{j=1}^{N_{\sin_\mu}{}^{i}} \sum_{k=1}^{N_{\sin_\nu}{}^{i}} k_{ijk}^{tc} \sin(n_j^i\phi_\mu - \gamma_j^i)\sin(m_k^i\phi_\nu - \gamma_k^i) \quad (41)$$

3. Computational Details

3.1. DFT Calculations. In all QM calculations the well tested density functional B3LYP method[46] with a correlation consistent basis set cc-pvDz was employed. For all tested molecules, the absolute energy minimum was obtained by a complete geometry optimization. Vibrational frequencies, gradients, and a Hessian matrix were computed from this optimized conformation. Torsional energy profiles for flexible molecules are obtained by performing calculations of the optimized energy without any restriction but the investigated "soft" IC, which was increased in a stepwise manner. All calculations were performed with the GAUSSIAN 03 package.[47]

3.2. Optimization of the FF Parameters. The program to compute the FF parameters through a fitting of the QM data was coded (in Fortran language) by the authors. It is coupled with the Gaussian 03 package for the input QM data, whereas the FF functions are read from a Moscito[48] input file. The output is again a Moscito input file which contains the optimized intramolecular input parameters. This program was named JOYCE in honor of the great Irish writer who spent many years in Italy. This program is free and can be obtained from the authors upon request.

3.3. Simulations. All MD simulations are carried out with a parallel version of the Moscito3.9[48] package. The equilibration runs are performed in the NPT ensemble on systems of 125 molecules at 298 K and 1 atm for at least 1 ns, keeping temperature and pressure constant using the weak coupling scheme of Berendsen et al.[49] The short-range intermolecular interactions are truncated at $R_c = 10$ Å, employing standard corrections for energy and virial.[1] Charge−charge long-range interactions are treated with the particle mesh Ewald (PME) method,[50,51] using a convergence parameter α of $5.36/2R_c$ and a fourth-order spline interpolation. In all cases the time step is set to 0.1 fs, since bond stretching is explicitly considered. An exception is made for the butoxybenzene molecule, where the bond lengths are kept fixed at their equilibrium value using the SHAKE algorithm[52] allowing a time step of 1 fs. After equilibration, NVE trajectories of 100 ps were produced in the NVE ensemble and used for the calculation of the velocity autocorrelation function

$$Z(t) = \langle v(t)\cdot v(0)\rangle \quad (42)$$

The latter is employed to obtain the power spectra as

$$P(\omega) = \frac{6}{\pi Z(0)}\int_0^{\infty} Z(t)\cos(\omega t)\mathrm{d}t \quad (43)$$

4. Results

4.1. Rigid Molecules. The first test was performed on four heterocyclic aromatic molecules, namely pyridine, furan, oxazole, and isoxazole. The Hessian matrix of each molecule, computed after DFT complete geometry optimization, was used to parametrize the intramolecular QMD-FF according to eq 13. Two different weighting factors W''_{KL} of 10^4 and 0.8×10^4 were used for the diagonal ($K = L$) and off-diagonal ($K \neq L$), respectively. Since all chosen molecules show rather stiff ICs we employed only the harmonic terms (36−38) in eq 35. It may be worth noticing that with this choice only one QM calculation (a complete optimization with frequencies) is needed to construct the QM database necessary for the intramolecular parametrization. A FA description was adopted as shown in Figure 1, and no restriction was imposed on the fitting parameters except those dictated by symmetry. All parameters were obtained with a standard deviation of $1.2-1.4 \times 10^{-2}$ kJ/mol and are reported in Tables 1−3, for stretching, bending, and torsions, respectively. For comparison, AMBER[14,17,53,54] parameters are also reported in the same tables.

By looking at Table 1, one can see that QMD and literature[53,54] stretching constants k^s are rather similar. Exceptions are those for the C−N bond in pyridine and the C−C in furan, which are found smaller by 25−30% in the QMD-FF.

For the bending constants k^b, reported in Table 2, the QMD parameters appear to retain a higher level of chemical specificity. Indeed, the QMD values indicate a marked difference between different bending motions, as for instance those regarding the C_N-N-C_N ($k^b = 569$ kJ/mol rad^{-2}) and the $N-C_N-C$ ($k^b = 869$ kJ/mol rad^{-2}) triplets in pyridine, which is not accounted for in the literature FF. Also in the

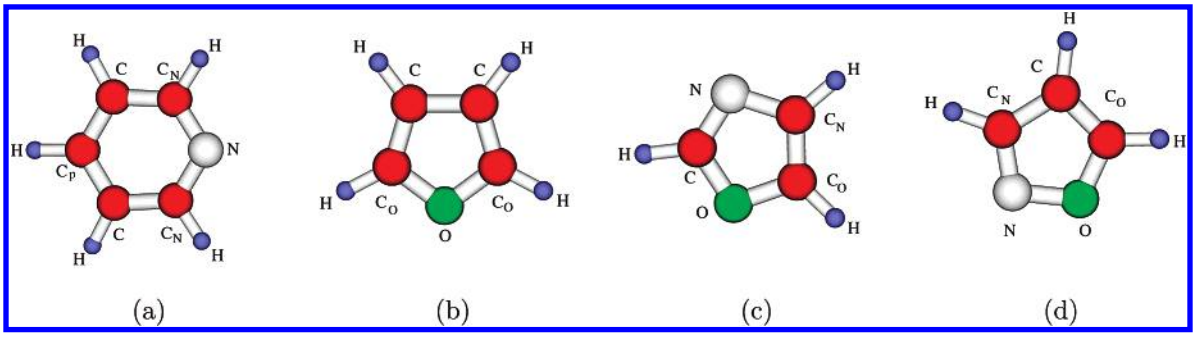

Figure 1. Test molecules in the FA models: (a) pyridine, (b) furan, (c) oxazole, and (d) isoxazole.

Table 1. QMD Fitted and AMBER[53,54] Parameters for Bond Stretching Potential of Eq 36[a]

pyridine				furan			
	k^s (kJ/mol Å^{-2})				k^s (kJ/mol Å^{-2})		
IC	QMD	AMBER	r_0 (Å)	IC	QMD	AMBER	r_0 (Å)
C_N-N	3036	4041	1.34	C_O-C	4133	4569	1.36
C_N-C	3132	3924	1.40	C−C	2793	3924	1.44
$C-C_p$	3398	3924	1.40	C_O-O	2921	2845	1.36
C*−H	3301	3071	1.09	C*−H	3497	3071	1.09
oxazole				**isoxazole**			
	k^s (kJ/mol Å^{-2})				k^s (kJ/mol Å^{-2})		
IC	QMD	AMBER	r_0 (Å)	IC	QMD	AMBER	r_0 (Å)
$O-C_O$	2836	2845	1.37	$O-C_O$	3147	2845	1.34
C_O-C_N	4067	4351	1.36	C_O-C	4090	4569	1.36
C_N-N	2904	3430	1.39	$C-C_N$	2789	3923	1.43
N−C	4433	4083	1.30	C_N-N	4028	3431	1.31
O−C	2535	3866	1.36	O−N	1884	3866	1.39
C*−H	3515	3071	1.09	C*−H	3485	3071	1.09

[a] Symbols refer to Figure 1; C* indicates every carbon atom in the ring. All the C*−H stretchings were constrained to the same value, since they resulted spontaneously very similar from the fitting procedure.

Table 2. QMD Fitted and AMBER[53,54] Parameters for Angle Bending Potential of Eq 37[a]

pyridine				furan			
	k^b (kJ/mol rad^{-2})				k^b (kJ/mol rad^{-2})		
IC	QMD	AMBER	θ_0 (deg)	IC	QMD	AMBER	θ_0 (deg)
$N-C_N-C$	869	586	124	C_O-C-C	708	586	106
$C-C_p-C$	637	527	120	$C-C_O-O$	641	586	111
C_N-N-C_N	569	586	117	C_O-O-C_O	796	586	107
C_p-C-C_N	596	527	120	-	-	-	-
$N-C_N-H$	392	293	116	$O-C_O-H$	324	293	116
C*−C *−H	314	293	120	C*−C*−H	240	293	127
oxazole				**isoxazole**			
	k^b (kJ/mol rad^{-2})				k^b (kJ/mol rad^{-2})		
IC	QMD	AMBER	θ_0 (deg)	IC	QMD	AMBER	θ_0 (deg)
$O-C_O-C_N$	767	586	108	$O-C_O-C$	582	586	110
C_O-C_N-N	838	586	109	C_O-C-C_N	731	586	103
C_N-N-C	729	586	104	$C-C_N-N$	762	586	113
O−C−N	889	586	115	$O-N-C_N$	873	586	105
C_O-O-C	846	586	104	C_O-O-N	970	586	109
$O-C_O-H$	386	293	116	$N-C_N-H$	308	293	118
N−C−H	234	293	129	$O-C_O-H$	321	293	116
O−C−H	345	293	117	$C-C_O-H$	254	293	134
$N-C_N-H$	395	293	122	C_O-C-H	254	293	129
C_O-C_N-H	151	293	129	C_N-C-H	254	293	128
C_N-C_O-H	151	293	135	$C-C_N-H$	254	293	119

[a] Symbols refer to Figure 1.

azoles, the bending constants involving hydrogen-containing triplets range from 151 kJ/mol rad^{-2} (C_O-C_N-H and C_N-C_O-H in oxazole) to 395 kJ/mol rad^{-2} ($N-C_N-H$ in oxazole), while the other triplets show force constants from 582 kJ/mol rad^{-2} ($O-C_O-C$ in isoxazole) to 970 kJ/mol rad^{-2} (C_O-O-N in isoxazole). Conversely literature FF only accounts for two types of constants, 293 and 586 kJ/mol rad^{-2}, depending on whether the triplet contains a hydrogen atom or not.

A similar comparison cannot be easily made with the torsion constants reported in Table 3, because different functional forms are used to describe "hard" dihedral motions. In particular the AMBER FF[14] does not distinguish between "hard" and "soft" dihedrals, employing sums of cosine functions even for the former type. However the QMD model should result in a lower tendency of the aromatic rings to lose planarity, since literature torsional constants never exceed 15 kJ/mol, and the employed sinusoidal functions[14] are much smoother than the harmonic model obtained in the present work and reported in Table 3.

According to eq 31, the intramolecular potentials described by the QMD and AMBER parameters were complemented with an intermolecular part, whose parameters were taken from an OPLS-FA description, explicitly designed to reproduce, through MC simulations in the liquid phase, some thermodynamic properties (as density or heat of vaporization) of the target molecules.[53,54] The resulting FFs, which will again be labeled QMD and AMBER for simplicity, were employed in MD simulations, according to the details given in the previous section. Two sets of MD simulations for each molecule were performed at 298 K and 1 atm; all systems were equilibrated for 1 ns, and thermodynamic averages were taken on production runs of a further ns.

From the average thermodynamic quantities reported in Table 4, it appears that the proposed QMD-FF well couples with the OPLS intermolecular parameters, since it does not alter the liquid density nor the energy distribution by more than 3%.

Moreover Figure 2, where the radial distribution functions $g(r)$ are reported for the oxygen−oxygen pair, shows that the liquid structure resulting from the QMD model is in excellent agreement with the AMBER results, retaining some

Table 3. Fitted Parameters for Dihedral Angles as in Eq 38[a]

pyridine			furan		
IC	k^t (kJ/mol rad^{-2})	ϕ_0	IC	k^t (kJ/mol rad^{-2})	ϕ_0
N−C_N−C−C $_p$	94	0	C_O−C−C−C_O	125	0
C_N−N−C_N−C	99	0	C−C_O−O−C_O	151	0
C−C_p−C−C_N	76	0	O−C_O−C−C	220	0
H−C−C_N−N	63	180	O−C_O−C−H	82	180
H−C_N−C−C_p	77	180	H−C_O−O−C_O	55	180
C_N−N−C_N−H	124	180	H−C−C−C_O	54	180
H−C−C_N−H	44	0	H−C−C−H	11	0
H−C_p−C−H	40	0	-	-	-
oxazole			**isoxazole**		
IC	k^t (kJ/mol rad^{-2})	ϕ_0	IC	k^t (kJ/mol rad^{-2})	ϕ_0
C−O−C_O−C_N	174	0	N−O−C_O−C	172	0
O−C_O−C_N−N	197	0	O−C_O−C−C_N	166	0
H−C_O−C_N−N	57	180	C_O−C−C_N−N	194	0
C_O−C_N−N−C	187	0	C−C_N−N−O	188	0
C_N−N−C−O	198	0	C_O−O−N−C_N	164	0
O−C_O−C_N−H	97	180	O−C_O−C−H	73	180
C_O−O−C−N	199	0	H−C−C_N−N	52	180
H−C_N−N−C	57	180	H−C_N−N−O	124	180
C−O−C_O−H	51	180	N−O−C_O−H	80	180
C_N −N−C−H	102	180	C_O−C−C_N−H	63	180
H−C_O−C_N −H	9	0	H−C*−C* −H	10	0
C_O−O−C−H	56	180	-	-	-

[a] Symbols refer to Figure 1; C* refers to any aromatic carbon atom.

Table 4. Thermodynamic Results Obtained for Rigid Molecules at 1 atm and 298 K Employing Both QMD and AMBER FFs

	QMD			AMBER		
molecule	density (g/cm ^{3})	E_{inter} (kJ/mol)	E_{intra} (kJ/mol)	density (g/cm ^{3})	E_{inter} (kJ/mol)	E_{intra} (kJ/mol)
pyridine	0.974 ± 0.006	−39.5	33.7	0.970 ± 0.006	−39.3	35.4
furan	0.970 ± 0.010	−27.7	26.7	0.944 ± 0.009	−26.6	26.8
oxazole	1.165 ± 0.010	−45.0	26.0	1.130 ± 0.008	−44.4	25.9
isoxazole	1.130 ± 0.006	−42.2	23.1	1.098 ± 0.008	−40.8	23.6

small differences between different azoles. It is also worth noticing that the computed functions are also in agreement with those reported in ref 54, where a OPLS/AMBER FF was used in MC simulations without including deformations of planarity and therefore involving no torsional energy term. Similar results are found with the several $g(r)$ functions of pyridine. Concerning with the internal structure, the QMD and AMBER distance and angle distributions are very similar both in position and shape. Small differences are instead found in the shape of the dihedral distributions, being that the QMD bands are more sharp and localized. This indicates an increased stiffness of the aromatic rings, in agreement with the higher value of the QMD torsional parameters reported in Table 3.

The good agreement in the considered structural and thermodynamic properties suggests that the representation of the molecular structure given by the atomistic QMD model is quite correct. This encouraged us to extend the present approach to UA parametrizations of larger, flexible molecules, which is the main scope of the present paper.

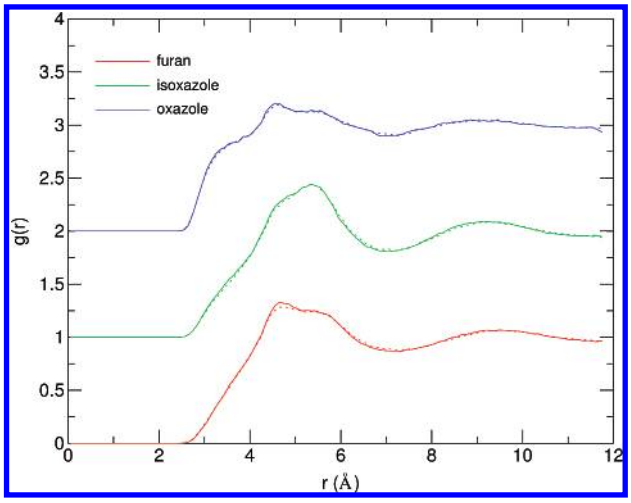

Figure 2. Oxygen−oxygen pair atomic correlation functions $g(r)$, computed for QMD-FF (solid lines) and for AMBER-FF (dashed lines). The isoxazole and oxazole curves are vertically shifted by 1 and 2, respectively.

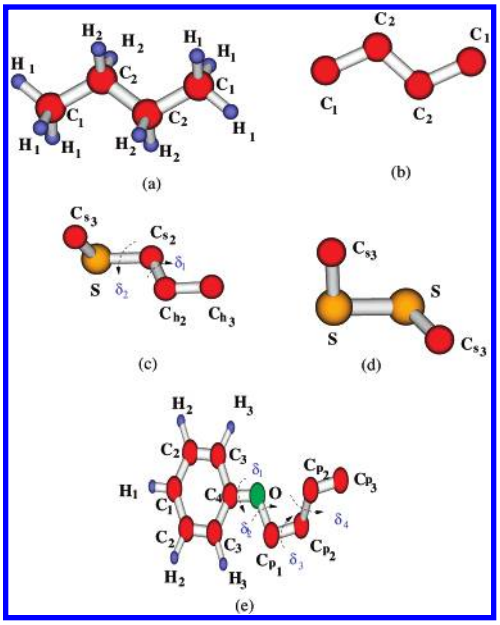

Figure 3. Test flexible molecules: (a) FA butane, (b) UA butane, (c) UA methyl propyl sulfide, (d) UA dimethyl disulfide, and (e) butoxybenzene.

4.2. Flexible Molecules and UA Description. Once the reliability of the QMD description of the molecular structure has been validated on rigid target molecules, the capability of the proposed method to describe the motion of "soft" ICs was tested on several molecules, namely *n*-butane, methyl-propyl sulfide, dimethyl disulfide, and *n*-butoxybenzene. The adopted models for these target molecules are reported in Figure 3. Panels (a) and (b) show the two different models (FA and UA, respectively) employed for *n*-butane, panels (c) and (d) report the UA models for methyl-propyl sulfide and dimethyl disulfide, while in panel (e) the "hybrid" model (FA for aromatic hydrogens and UA for the aliphatic lateral chain) was employed for *n*-butoxybenzene.

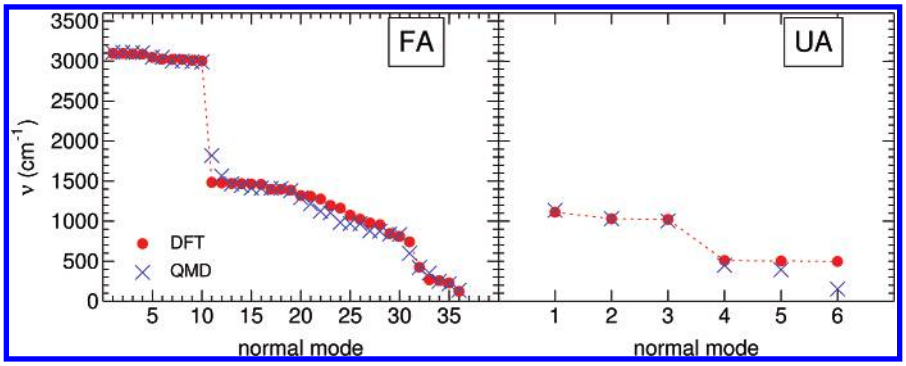

Figure 4. Normal modes frequencies computed by (red full circles) and predicted by the QMD-FF (blue crosses) for the butane molecule in the FA (left panel) and UA (right panel) model.

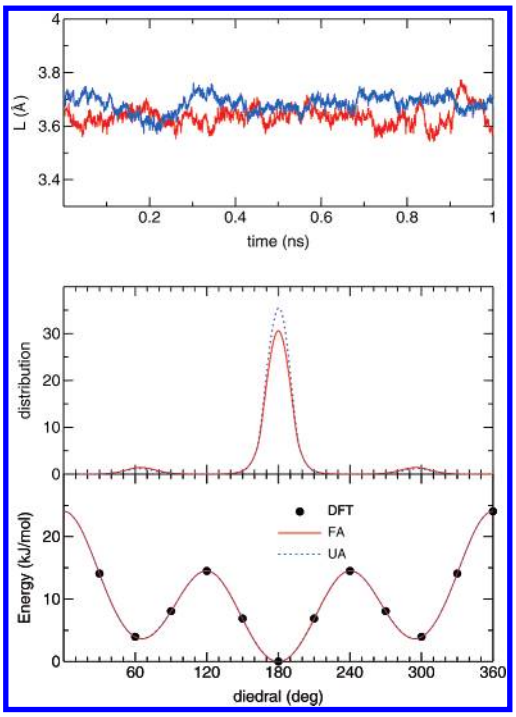

Figure 5. $C_1-C_2-C_2-C_1$ butane's dihedral in FA and UA models. Bottom panel: dihedral energy profile computed with DFT (black full circles) and QMD FA (red solid line) and UA (blue dashed line) potentials. Middle panel: dihedral distributions at 298 K and 1 atm computed in 1 ns FA (red) and UA (blue) models. Upper panel: butane elongation ($L = C_1-C_1$ distance) vs simulation time. Red and blue lines again refer to FA and UA models, respectively.

The energy profile exhibited by the "soft" degrees of freedom is rather flat and exhibits several local minima (see bottom panel of Figure 5) so that strongly distorted conformations may be populated, even at room temperature. This causes the equilibrium geometry and the related vibrational frequencies not to furnish sufficient data to parametrize the torsional potential, and several energy calculations at different geometries are needed to take into account large amplitude motions. Nevertheless, by imposing W' and W'' in eq 13 to be zero for each geometry different from the equilibrium one, the computational cost of the QM calculations is still reduced, since no vibrational frequency is needed except those in the minimum energy configuration. The inclusion of distorted geometries obtained by sampling the intramolecular energy surface imposing different values of the investigated "soft" dihedral and relaxing the other ones presents however some problems which may be clarified through a simple example.

The *n*-butane molecule in the UA approach (Figure 4, panel (b)) has six ICs: three bond distances, two bond angles, and one dihedral. The latter has to be considered as a "soft" IC. Let us suppose that the fitting includes two conformations, namely the staggered equilibrium ($C_1-C_2-C_2-C_1 = 180°$) and eclipsed ($C_1-C_2-C_2-C_1 = 0°$) whose relative energy E(eclip) − E(stagg) is 24 kJ/mol. The central C_2-C_2 distance is different for the two conformations 2.90 Å and 2.95 Å, respectively, for the staggered and eclipsed, whereas the two bending angles change by about 3°. Despite the dihedral angle being by far the most evident geometrical change on going from staggered to eclipsed conformation, relevant energy contributions occur even for the small changes of the other ICs: bond lengths and angles account for 3.4 and 2.9 kJ/mol, respectively. Consequently the torsional energy term of eq 39 accounts for about 75% of the relative energy E(eclip) − E(stagg). Therefore the resulting pure torsional potential (eq 39) describes a lower barrier (18 rather than 24 kJ/mol), being the remaining gap accounted for the energy terms of the bond distances and angles.

This (rather obvious) finding has the unpleasant consequence that a good description of the large amplitude torsional geometrical movements cannot be achieved with high accuracy by simple FFs. Indeed, by using a class I FF (i.e., no coupling term), the fraction of the torsional energy connected with the changes of the other IC is completely lost, because there is no reason for the bond lengths and angles to change during the internal rotation (frozen rotation). In fact the information linking the dihedral to the other ICs in the QM calculation is completely lost, since in central FFs the motion of one IC is independent from the value of the other ICs. The straightforward remedy for this problem would require the inclusion of a relevant number of coupling functions in eq 40, as done for example in the QMFF procedure,[29] with the consequence of increasing the number of functions in the FF. A more simple and direct solution is to ignore the changes of most of the ICs not directly involved in the internal rotation and, in case, retaining the changes of few pertinent ICs whose coupling terms with the dihedral are included in the FF. This route has the effect of ascribing

Table 5. Fitted Parameters for the Bond Stretching Potential of Eq 36 Computed for FA and UA Butane, Employing the FIRA[a]

model	IC	k^s (kJ/mol Å^{-2})	r_0 (Å)
FA	C_1-C_2	2249	1.53
UA	C_1-C_2	2594	1.53
FA	C_2-C_2	2146	1.53
UA	C_2-C_2	2353	1.53
FA	C_1-H_1	3101	1.10
FA	C_2-H_2	2996	1.11

[a] Symbols refer to panels (a) and (b) of Figure 4.

Table 6. Fitted Parameters for the Angle Bending Potential of Eq 37, Computed for FA and UA Models of Butane with the FIRA[a]

model	IC	k^b (kJ/mol rad^{-2})	θ_0 (deg)
FA	$C_1-C_2-C_2$	743	113
UA	$C_1-C_2-C_2$	927	113
FA	$C_2-C_1-H_1$	342	112
FA	$C_1-C_2-H_2$	401	110
FA	$C_2-C_2-H_2$	396	109
FA	H*−C*−H*	334	106

[a] Symbols refer to panels (a) and (b) of Figure 4; C* and H* indicate every carbon and hydrogen atom in the ring, respectively.

Table 7. Fitted Parameters for Dihedral Angles of FA and UA Models of Butane as Defined in Eq 39 in the FIRA[a]

FA									UA		
$C_1-C_2-C_2-C_1$			*−$C_2-C_2-H_2$			H−C_1-C_2−*			$C_1-C_2-C_2-C_1$		
k^d (kJ/mol)	n	γ	k^d (kJ/mol)	n	γ	k^d (kJ/mol)	n	γ	k^d (kJ/mol)	n	γ
−14.132	0	0	-	0	0	-	0	0	−2.106	0	0
4.349	1	0	-	1	0	-	1	0	4.330	1	0
1.737	2	0	-	2	0	-	2	0	1.738	2	0
0.847	3	0	0.847	3	0	0.712	3	0	7.520	3	0
1.629	4	0	1.629	4	0	-	4	0	0.126	4	0
1.052	5	0	1.052	5	0	-	5	0	0.172	5	0
0.029	6	0	0.029	6	0	-	6	0	0.241	6	0

[a] Symbols refer to panels (a) and (b) of Figure 4; C*, H*, and * indicate any carbon, hydrogen, and carbon or hydrogen atoms, respectively.

the torsional energy to the torsional term (39) only, whereas in the QM calculation it is distributed on several ICs since all the ICs are in principle coupled to each other. This method, which has been implicitly adopted in partial parametrization of flexible molecules[24,35,38] will be called FIRA: frozen internal rotation approximation.

4.3. The UA Prototype: *n*-Butane. The parameters for both FA and UA descriptions of the *n*-butane molecule (reported in Tables 5−7) were obtained through eq 13 by choosing $W = 1$ for each energy, $W' = 0$ for each gradient, and $W''_{KL} = 1 \times 10^4$ and 0.5×10^4 for the diagonal ($K = L$) and off-diagonal ($K \neq L$) terms of the Hessian matrix in the equilibrium geometry. For all distorted geometries W'' was set to be null.

The torsional potentials around the C_1-C_2 and C_2-C_2 bonds were sampled with 7 points in the 0−180° range, but obviously only the latter was used to obtain the parameters in the UA description. By comparing the stretching and bending constants of the two models, reported in Tables 5 and 6, it appears that the increased size of the UA interaction sites shifts the k's to higher values. Conversely, the torsion around the C_2-C_2 bond, reported in Table 7, is described by almost the same FA and UA parameters, with the only exception of the $n = 0$ constant term, which does not alter the shape of the potential curve.

The comparison between DFT and QMD vibrational frequencies, reported in Figure 4, clearly shows that the proposed procedure is capable of removing the high frequencies from the FA description (i.e., those due to C−H stretching and bendings) and reproducing with good approximation those remaining in the UA molecule. An exception is made by the last UA normal mode, which essentially involves the low frequency torsion of the $C_1-C_2-C_2-C_1$ dihedral. However the energy profile of such torsion, reported in the bottom panel of Figure 5, is well represented by the two models, making us confident that the QMD potentials will be able to reproduce the correct population distribution for *n*-butane.

Simulations were carried out for both FA and UA models at 298 K and 1 atm, equilibrating the systems for almost 2 ns. Intermolecular interactions were modeled with the OPLS-AA[15,55] and UA[56] FF parameters for *n*-butane. The resulting average densities of 0.555 g/cm^3 and 0.584 g/cm^3, obtained for FA and UA models respectively, well agree with both recent MC simulation results (0.558 g/cm^3) and the experimental value of 0.5729 g/cm^3 (see ref 55 and references therein); the radial distribution functions, computed for both models, did not show any marked difference. The heats of vaporization (ΔH_{vap}), computed as suggested in refs 31, 55, and 56, are in good agreement with both OPLS-AA (5.00 kcal/mol) and experimental values (5.04 kcal/mol, see ref 55 and references therein), being 5.02 kcal/mol and 5.09 kcal/mol for QMD-FA and QMD-UA, respectively. The distribution of the $C_1-C_2-C_2-C_1$ dihedral and the time evolution of the end-to-end chain elongation L, reported in Figure 5, confirm the capability of the QMD-UA FF to account for the correct molecular structure for an aliphatic flexible chain. Indeed, the average L values of 3.64 Å and 3.68 Å, obtained for the FA and UA models, are very similar to recent MC results (3.67 Å), reported for liquid *n*-butane at the same temperature.

4.4. Two Sulfur Containing Molecules. The next two molecules considered to test the UA approximation are methyl-propyl sulfide (MPS) and dimethyl disulfide (DMDS), respectively, reported on panels (c) and (d) of Figure 3. The UA approximation implies that all methylene and methyl groups are treated as a single site coincident with the involved carbon atom. The parameters for both these molecules were obtained through the fitting by applying the same procedure and weights of the *n*-butane molecule: the resulting values are reported in Tables 8 and 9.

In the bottom panels of Figure 6 (a),(b), the resulting torsional potentials are compared to the computed energy data, for MPS and DMDS, respectively. It appears that the adoption of the UA model, in the FIRA approximation, does not alter the main features of the QM torsional curves. In particular the 90° minimum for the DMDS dihedral is well reproduced, and the small differences between the potential

Table 8. Fitted Parameters for Bond Stretching (Eq 36) and for Angle Bending (Eq 37) for UA Methyl-Propyl Sulfide (MPS) and Dimethyl Disulfide (DMDS), Employing the FIRA[a]

MPS			DMDS		
IC	k^s (kJ/mol Å^{-2})	r_0 (Å)	IC	k^s (kJ/mol Å^{-2})	r_0 (Å)
$C_{h3}-C_{h2}$	2476	1.53	$C_{s3}-S$	1697	1.84
$C_{h2}-C_{s2}$	2404	1.53	S−S	1217	2.09
$C_{s2}-S$	1424	1.84	-	-	-
$S-C_{s3}$	1728	1.83	-	-	-

MPS			DMDS		
IC	k^b (kJ/mol rad^{-2})	θ_0 (deg)	IC	k^b (kJ/mol rad^{-2})	θ_0 (deg)
$C_{h3}-C_{h2}-C_{s2}$	1013	112	$C_{s3}-S-S$	1086	103
$C_{h2}-C_{s2}-S$	724	115	-	-	-
$C_{s2}-S-C_{s3}$	2290	101	-	-	-

[a] Symbols refer to panels (c) and (d) of Figure 3.

Table 9. Fitted Parameters for Dihedral Torsion Potential of Eq 39 Computed for UA Methyl-Propyl Sulfide (MPS) and Dimethyl Disulfide (DMDS), Employing the FIRA[a]

	MPS		DMDS
n	δ_1 k^d (kJ/mol)	δ_2 k^d (kJ/mol)	$C_{s3}-S-S-C_{s3}$ k^d (kJ/mol)
0	−2.899	−2.899	−5.069
1	4.070	3.604	6.010
2	2.404	3.263	16.805
3	7.462	4.194	3.219
4	0.017	0.012	0.342
5	0.036	0.096	0.263
6	0.181	0.130	0.045

[a] Symbols refer to panels (c) and (d) of Figure 3.

Table 10. Thermodynamic Properties of MPS and DMDS[a]

	MPS			DMDS		
	QMD-UA	OPLS-UA	exp	QMD-UA	OPLS-UA	exp
ρ (g/cm^3)	0.822	0.796	0.837	1.009	1.031	1.057
ΔH_{vap} (kJ/mol)	29.3	26.7	31.8	38.0	38.8	38.4

[a] OPLS and experimental values are reported in ref 57.

energy curves with respect to dihedrals δ_1 and δ_2 of MPS are also retained.

MD simulations were performed by adding the OPLS intermolecular parameters designed for liquid sulfur compounds.[57] In this way the QMD and OPLS FFs differ for the intramolecular part, and a comparison of the results may give an indication as to the quality of our QMD FF. All simulations were carried out at 298 K and 1 atm, equilibrating both MPS and DMS systems for more than 2 ns.

In Figure 6 the resulting dihedral distributions are reported in the top of panel (a) and (b) for MPS and DMDS, respectively. It is worth noticing that both curves agree well with those reported in ref 57, where OPLS parameters were designed, confirming that the QMD UA approach can provide a correct sampling of the molecular configurations assumed in the condensed phase. Turning to the thermodynamic properties, it is apparent from Table 10 that the QMD results are in very good accord with both the OPLS and the experimental ones. It is fair to stress that the accuracy of the heats of vaporizations must be mainly ascribed to the

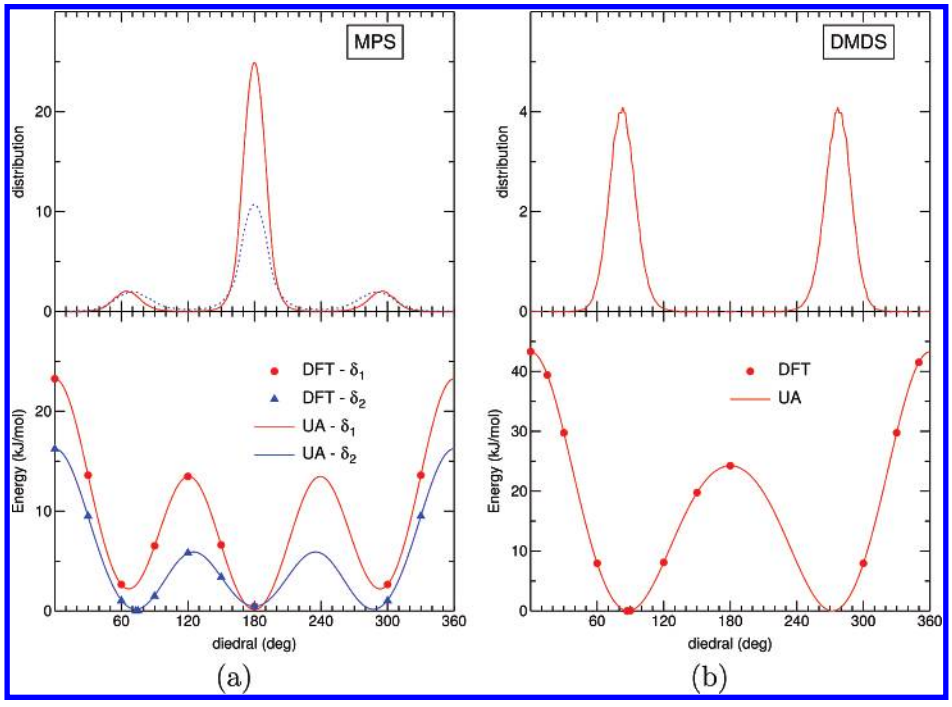

Figure 6. MPS and DMDS dihedrals. Bottom panels: (a) MPS dihedral energy profile computed with DFT (circles) and QMD UA potentials (solid line) for dihedrals δ_1 (red) and δ_2 (blue) of Figure 3 and (b) DMDS dihedral energy profile computed with DFT (circles) and QMD UA potentials (solid line). Top panels: (a) dihedral distributions at 298 K and 1 atm computed in 1 ns for dihedrals δ_1 (red line) and δ_2 (blue line) of MPS and (b) dihedral distributions at 298 K and 1 atm computed in 1 ns for DMDS dihedral.

Table 11. Fitted Parameters for Angle Bending Potential of Eq 37 Obtained for Both Coupled and Uncoupled Models of Butoxybenzene[a]

IC	k^b (kJ/mol rad^{-2})	θ_0 (deg)
C*−C*−C*	641	120
C*−C*−H*	320	120
C_3-C_4-O	786	120
C_4-O-C_{p1}	315	119
$O-C_{p1}-C_{p2}$	1548	108
$C_{p1}-C_{p1}-C_{p2}$	1071	114
$C_{p2}-C_{p2}-C_{p3}$	969	113

[a] Symbols refer to panel (e) of Figure 3; C* and H* stand for any aromatic carbon or hydrogen, respectively.

Table 12. Fitted Parameters for Dihedral Harmonic Torsional Potential of Eq 38 Obtained for Both for Coupled and Uncoupled Models of Butoxybenzene[a]

IC	k^t (kJ/mol rad^{-2})	ϕ_0 (deg)
C*−C*−C*−C*	82	0
C*−C*−C*−H*	66	180
H*−C*−C*−H*	40	0
H*−C*−C*−O	43	0
C*−C*−C*−O	159	180

[a] Symbols refer to panel (e) of Figure 3; symbols C* and H* stand for any aromatic carbon or hydrogen, respectively.

Table 13. Fitted Parameters for Dihedral Angles of Butoxybenzene of Butane as Defined in Eq 39

δ_1 ($C_3-C_4-O-C_{p1}$)				δ_2 ($C_4-O-C_{p1}-C_{p2}$)			
n	γ	k^d (kJ/mol) uncoupled model	k^d (kJ/mol) coupled model	n	γ	k^d (kJ/mol) uncoupled model	k^d (kJ/mol) coupled model
0	0	0.557	0.794	0	0	0.279	0.397
2	0	−3.165	−2.924	1	0	12.387	8.679
4	0	−0.344	−0.543	2	180	−5.271	−2.587
6	0	0.275	0.120	3	0	6.735	4.356
-	-	-	-	4	180	0.299	0.356
-	-	-	-	5	0	0.045	0.008
-	-	-	-	6	180	−0.674	−0.388

δ_3 ($O-C_{p1}-C_{p2}-C_{p2}$)				δ_4 ($C_{p1}-C_{p2}-C_{p2}-C_{p3}$)			
n	γ	k^d (kJ/mol) uncoupled model	k^d (kJ/mol) coupled model	n	γ	k^d (kJ/mol) uncoupled model	k^d (kJ/mol) coupled model
0	0	0.279	0.397	0	0	0.279	0.397
1	0	1.889	1.970	1	0	3.676	3.641
2	0	2.374	2.359	2	0	1.855	1.609
3	0	7.882	7.785	3	0	7.035	6.775
4	0	0.346	0.470	4	0	0.198	0.119
5	0	−0.139	0.066	5	0	0.605	0.396
6	0	0.113	−0.378	6	0	0.456	0.386

excellent capability of the intermolecular OPLS parameters to reproduce this quantity.

4.5. *n*-Butoxybenzene. The last target molecule *n*-butoxybenzene contains a rigid aromatic ring linked to a flexible aliphatic chain, a chemical situation frequently found in many liquid crystals and molecules of biological interest. In the adopted model, all aromatic hydrogen atoms were taken explicitly into account, while the methyl and methylene groups of the chain were modeled in a UA description, as shown in panel (e) of Figure 3. As done for butane, torsional energy profiles of each of the four dihedrals ($\delta_1-\delta_4$) were sampled with 8 points in the 0−180° range. All these calculations, together with the optimized geometry and frequencies, were used in the fitting procedure, with the same weighting factors reported for butane. The resulting parameters are reported in Tables 11−14. Since in preliminary fittings it was noted that the force constants of the "hard" ICs did not change significantly in going from the uncoupled to the coupled model, for the sake of simplicity all k^b and k^t of the coupled model were constrained to their uncoupled value during the fitting.

Table 14. Fitted Parameters for Dihedral Couplings in Butoxybenzene Coupled Model as Defined in Eq 41

IC 1	IC 2	n	γ	m	α	k^{tc} (kJ/mol)
δ_1	δ_2	2	0	1	0	−1.1613
δ_1	δ_3	2	0	1	0	−0.1205
δ_2	δ_3	1	0	1	0	−0.9943

By looking at Tables 11 and 12, one can see as the bending and the "hard" torsion constants assume a broad range of values: 315−1548 and 40−159 J/mol rad^{-2}, respectively. This is not obvious since the atom triplets or quartets may be very similar at first sight. This may be regarded as further proof of QMD's capability to capture subtle different behavior of the ICs involving similar atom types. It is also important to point out that similar ICs belonging to different molecules result in similar parameters without

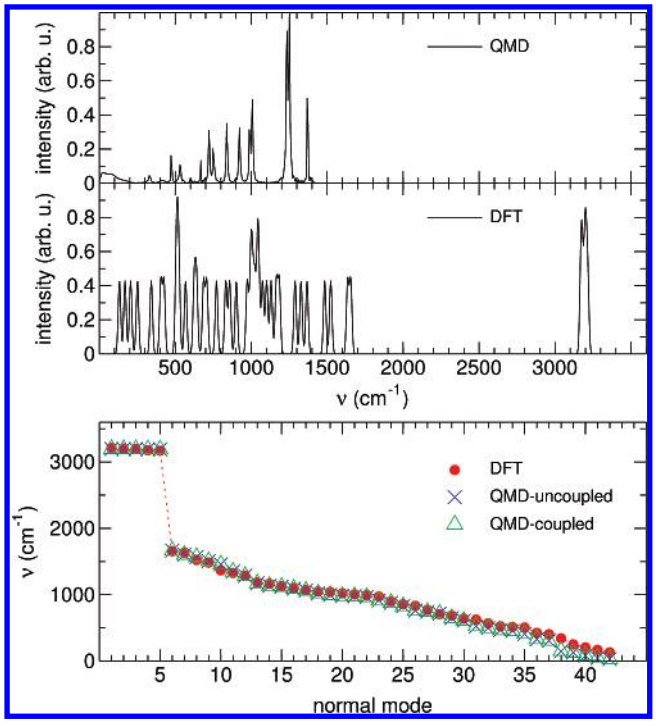

Figure 7. Vibrational modes of butoxybenzene. Bottom panel: comparison between DFT frequencies (red full circles) computed in the UA approximation according to eqs 28 and 29 and QMD predicted frequencies in the uncoupled (blue crosses) and coupled (green triangles) models. Upper panel: DFT computed power spectrum (bottom) and MD computed power spectrum at 298 K and 1 atm.

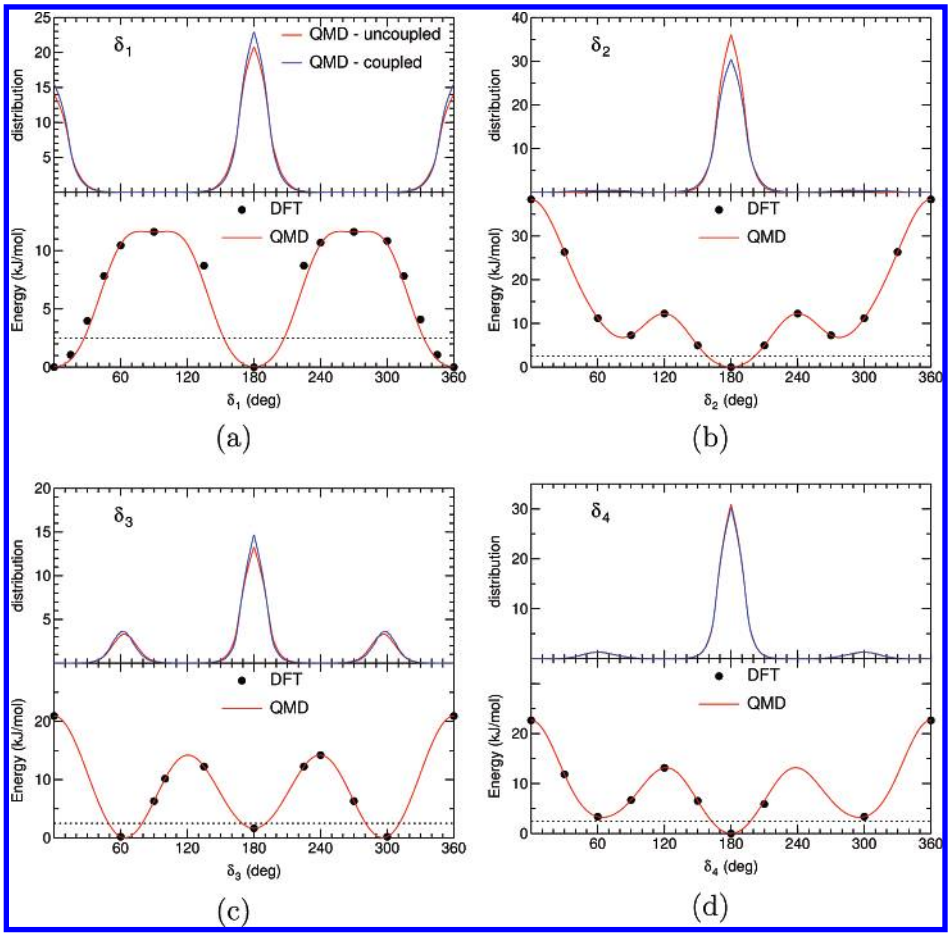

Figure 8. Dihedral potentials and distributions for butoxybenzene. DFT computed energies and uncoupled QMD FF are reported in bottom subpanels of panels (a)−(d) for dihedrals $\delta_1-\delta_4$. Black dotted lines indicate the thermal energy at 298 K. In the upper subpanels are reported dihedral distributions computed from the MD trajectories produced with the uncoupled (red lines) and coupled QMD-FFs.

having imposed any constraint, as the bending constants of butane ($C_1-C_2-C_2$, 927 kJ/mol rad^{-2}) and butoxybenzene ($C_{p2}-C_{p2}-C_{p3}$, 969 kJ/mol rad^{-2}) or the "hard" dihedral constants of pyridine ($H-C-C_N-H$, 42 kJ/mol rad^{-2}) and butoxybenzene (H*−C*−C*−H*, 40 kJ/mol rad^{-2}). This seems to indicate that a certain level of transferability does exist, though this is to be verified depending on the molecule under study.

With regards to the torsional potentials, two different models have been adopted: an uncoupled and a coupled one (see eq 41), whose parameters are reported in Tables 13 and 14. The δ_4 dihedral was not coupled to the other dihedrals, and the parameters driving its torsion are slightly affected by the inclusion of the coupling terms between the other dihedrals. Conversely the inclusion of couplings between δ_1, δ_2, and δ_3 causes some changes in the parameters on the pure torsional terms (39), despite the low value of the coupling parameters $\simeq$ 1 kJ/mol.

The effect of the coupling on the resulting frequencies is almost negligible, as shown in the bottom panel of Figure 7, and the agreement with the DFT computed vibrational frequencies is good for both models. It is worth noticing the absence, in both coupled and uncoupled models, of nonbonded interactions between sites which are separated by more than four bonds, as for example the methyl group C_{p3} and the carbon atoms of the ring. In fact the presence of these terms couples all the ICs involving the two sites affected by the nonbonded interactions, introducing off diagonal elements which are not easily controlled during the fitting. Therefore we have chosen to include such terms only when strictly necessary, to prevent, for example, unphysical "curling" of the aliphatic chain over the ring. Due to the relative short length of the butoxybenzene chain, this was found to never be the case. However for longer chain lengths, as for example in the alkyl cyanobiphenyl series (with $n > 4$), where nonbonded interactions between chain sites and aromatic rings have been found to be necessary, a simple method of introducing them has been devised in our laboratory.[23,24,26]

The coupled and uncoupled sets of intramolecular parameters obtained for butoxybenzene were complemented with the OPLS[15] intermolecular parameters, and MD simulations were performed at 298 K and 1 atm. Owing to the increase of molecular dimensions and, consequently, to the time range needed for phase equilibration, it would be preferable to augment the equilibration time to at least 5 ns. To maintain the computational expense acceptable, the time step was increased to 1 fs, and energy conservation was ensured by constraining the stretching motions to equilibrium value during the simulations. The consequence of this choice are

evident in the upper panel of Figure 7, where the power spectrum resulting from MD runs is compared to that predicted by the DFT calculations: the agreement is satisfactory for all frequencies except those corresponding to aromatic C−H stretching or C−C skeletal bands, which obviously disappear in the constrained simulation run.

Finally the effect of the coupling terms was checked on the dihedral's average distributions, along the MD trajectories. In Figure 8 the energy profiles and the dihedral distributions are reported for both uncoupled and coupled models. The effect of the coupling terms is negligible on the vibrational frequencies but alters the dihedral distributions of δ_1 and δ_2, which are the most coupled dihedrals. However, the differences in distribution are rather small, since the couplings between butoxybenzene's dihedrals are best appreciated in high-energy unfavorable conformations, which are not populated at room temperature.

5. Conclusions

An intramolecular parametrization of FFs, suitable for molecular simulations of condensed phase and based only upon QM calculations, is proposed here and validated. The main scope of the present work is not to provide general force fields to be put in standard MD packages but rather to implement a method which everyone can use in order to obtain a specific FF for the molecule under study. With this aim the present method has been implemented through the JOYCE program, a user-friendly Fortran code written by the authors and available upon request.

As a first benchmark, a group a rigid heteroaromatic molecules was chosen, whose description through literature FFs has shown to be accurate. The comparison of MD simulation results obtained with both the standard FF and the quantum mechanically derived (QMD) is favorable.

However the main scope of the proposed approach, rather than yielding very accurate FFs for small rigid molecules, is to provide intramolecular FFs for large (and often flexible) molecules, whose bonded parameters are less transferable or even not reported in the literature. For these reasons we have tested the QMD parametrizations on medium-size flexible molecules, modeled through representations of different complexity. Particular attention has been paid to the possibility of parametrizing bonded interaction between coarse grained sites grouping more than one atom, in view of applications to MD simulations of advanced materials condensed phases. In this sense *n*-butane can be seen as the smallest prototype of longer alkyl chains, which can be found in many liquid crystals or polymers. FA and UA reported parametrizations, employed in MD simulations, have shown that the QMD procedure is capable of reproducing many results achieved with widely employed literature FFs. Similar good results are then obtained for two sulfur containing molecules, again using the UA approach.

Finally the method was tested on *n*-butoxybenzene, a nonstandard molecule, whose intramolecular parameters (in particular those regarding the alkoxyl-aryl dihedral) are not readily available in literature databases. Also in this case the QMD-FF yields satisfactory results for dihedral distributions and vibrational frequencies which are in good agreement with the DFT values.

The present results have encouraged us to apply the reported procedure to some large liquid crystals forming molecules. The obtained QMD intramolecular potentials will be joined with intermolecular FFs produced through the FRM approach, recently devised in our group to compute the interaction energy between two large molecules. In fact it is worth pointing out that the proposed intra- and interparametrization procedure can be applied to any target molecule, regardless of its dimensions. In such a way the whole FF is obtained by a first principles approach, without the aid of any experimental data. This will allow us to perform MD or MC simulations with FFs specifically suited on the target molecules, thus accomplishing an important step toward predictivity. Such calculations are currently in progress in our laboratory.

References

(1) Allen, M.; Tildesley, D. *Computer Simulation of Liquids;* Clarendon: Oxford, U.K., 1987.

(2) Frenkel, D.; Smith, B. *Understanding Molecular Simulations;* Academic Press: San Diego, CA, 1996.

(3) Chávez-Páez, M.; dePablo, L.; dePablo, J. *J. Chem. Phys.* **2001**, *114*, 10948.

(4) Hackett, E.; Manias, E.; Giannelis, E. *Chem. Mater.* **2000**, 12, 2161.

(5) Colmenero, J.; Alvarez, F.; Arbe, A. *Phys. Rev. E* **2002**, *65*, 041804.

(6) Harmandaris, V.; Mavrantzas, V.; Theodorou, D.; Kroeger, M.; Ramirez, J.; Oettinger, H.; Vlassopoulos, D. *Macromolecules* **2003**, 36, 1376.

(7) *Computer Simulations of Liquid Crystals and Polymers NATO ASI series;* Pasini, P., Zannoni, C., Zumer, S., Eds.; Kluwer: Dordrecht, 2005.

(8) Care, C.; Cleaver, D. *Rep. Prog. Phys.* **2005**, *68*, 2665.

(9) Wohlert, J.; Olle, E. *J. Chem. Phys.* **2006**, *125*, 204703.

(10) Müller, M.; Katsov, K.; Schick, M. *Phys. Rep.* **2006**, *434*, 113.

(11) Brooks, B. R.; Bruccoeri, R. E.; Olafson, B. D.; States, D. J.; Swaminanthan, S.; Karplus, M. *J. Comput. Chem.* **1983**, *4*, 187.

(12) Halgren, T. *J. Comput. Chem.* **1996**, *17*, 490.

(13) Hermans, J.; Berendsen, H.; van Gusteren, W.; Postma, J. *Biopolymers* **1984**, *23*, 1.

(14) Cornell, W.; Cieplak, P.; Bayly, C.; Gould, I.; Merz, K.; Ferguson, D.; Spellmeyer, D.; Fox, T.; Caldwell, J.; Kollmann, P. *J. Am. Chem. Soc.* **1995**, *117*, 5179.

(15) Jorgensen, W.; Maxwell, D.; Tirado-Rives, J. *J. Am. Chem. Soc.* **1996**, *118*, 11225.

(16) Damm, W.; Frontera, A.; Tirado-Rives, J.; Jorgensen, W. *J. Comput. Chem.* **1997**, *18*, 1955.

(17) Wang, J.; Wolf, R.; Caldwell, J.; Kollman, P.; Case, D. *J. Comput. Chem.* **2004**, *25*, 1157.

(18) Zannoni, C. *J. Mater. Chem.* **2001**, *11*, 2637.

(19) Voth, G. A. *J. Chem. Theory Comput.* **2005**, *2*, 463.

(20) Yang, L.; Tan, C.; Hsieh, M.; Wang, J.; Duan, Y.; Cieplak, P.; Caldwell, J.; Kollmann, P.; Luo, R. *J. Phys. Chem. B* **2006**, *110*, 13166.

(21) Amovilli, C.; Cacelli, I.; Campanile, S.; Prampolini, G. *J. Chem. Phys.* **2002**, *117*, 3003.

(22) Amovilli, A.; Cacelli, I.; Cinacchi, G.; De Gaetani, L.; Prampolini, G.; Tani, A. *Theor. Chim. Acc.* **2007**, *117*, 885.

(23) Bizzarri, M.; Cacelli, I.; Prampolini, G.; Tani, A. *J. Phys. Chem. A* **2004**, *108*, 10336.

(24) Cacelli, I.; Prampolini, G.; Tani, A. *J. Phys. Chem. B* **2005**, *109*, 3531.

(25) De Gaetani, L.; Prampolini, G.; Tani, A. *J. Phys. Chem. B* **2006**, *110*, 2847.

(26) Cacelli, I.; De Gaetani, L.; Prampolini, G.; Tani, A. *J. Phys. Chem. B* **2007**, *111*, 2130.

(27) Prampolini, G. *J. Chem. Theory Comput.* **2006**, *2*, 556.

(28) Maple, J.; Dinur, U.; Hagler, A. *Proc. Natl. Acad. Sci. U.S.A.* **1988**, *85*, 5350.

(29) Maple, J.; Hwang, M.-J.; Stockfish, T.; Dinur, U.; Waldman, M.; Ewig, C.; Hagler, A. *J. Comput. Chem.* **1994**, *15*, 162.

(30) Palmo, K.; Mannfors, B.; Mirkin, N.; Krimm, S. *Biopolymers* **2003**, *68*, 383.

(31) Kaminski, G.; Jorgensen, W. *J. Phys. Chem.* **1996**, *100*, 18010.

(32) Dasgupta, S.; Brameld, K.; Fan, C.-F.; Goddard, W., III *Spectrochim. Acta, Part A* **1997**, *53*, 1347.

(33) Chelli, R.; Cardini, G.; Procacci, P.; Righini, R.; Califano, S. *J. Chem. Phys.* **2000**, *113*, 6851.

(34) Gontrani, L.; Ramondo, F.; Caminiti, R. *Chem. Phys. Lett.* **2006**, *422*, 256.

(35) Adam, C.; Clark, S.; Wilson, M.; Ackland, G.; Crain, J. *Mol. Phys.* **1998**, *93*, 947.

(36) Namba, A.; Léon, S.; da Silva, G.; Alemán, C. *J. Comput.-Aided Mol. Des.* **2001**, *15*, 235.

(37) Ceccarelli, M.; Procacci, P.; Marchi, M. *Comput. Mater. Sci.* **2001**, *20*, 318.

(38) Berardi, R.; Muccioli, L.; Zannoni, C. *ChemPhysChem.* **2004**, *5*, 104.

(39) LaPenna, G.; Catalano, D.; Veracini, C. A. *J. Chem. Phys.* **1996**, *105*, 7097.

(40) Dasgupta, S.; Yamasaki, T.; Goddard, W., III *J. Chem. Phys.* **1996**, *104*, 2898.

(41) Pulay, P.; Fogarasi, G. *J. Chem. Phys.* **1992**, *96*, 2856.

(42) Peng, C.; Ayala, P.; Shlegel, H.; Frisch, M. *J. Comput. Chem.* **1996**, *17*, 49.

(43) Dasgupta, S.; Goddard, W., III *J. Chem. Phys.* **1989**, *90*, 7207.

(44) Bakken, V.; Helgaker, T. *J. Chem. Phys.* **2002**, *117*, 9160.

(45) Press, W.; Teukolsky, S.; Vetterling, W.; Flannery, B. *Numerical Recipies in Fortran 77;* Cambridge University Press: Cambridge, U.K., 1992.

(46) Becke, A. *J. Chem. Phys.* **1993**, *98*, 5648.

(47) Frisch, M. J.; Trucks, G. W.; Schlegel, H. B.; Scuseria, G. E.; Robb, M. A.; Cheeseman, J. R.; Montgomery, J. A., Jr.; Vreven, T.; Kudin, K. N.; Burant, J. C.; Millam, J. M.; Iyengar, S. S.; Tomasi, J.; Barone, V.; Mennucci, B.; Cossi, M.; Scalmani, G.; Rega, N.; Petersson, G. A.; Nakatsuji, H.; Hada, M.; Ehara, M.; Toyota, K.; Fukuda, R.; Hasegawa, J.; Ishida, M.; Nakajima, T.; Honda, Y.; Kitao, O.; Nakai, H.; Klene, M.; Li, X.; Knox, J. E.; Hratchian, H. P.; Cross, J. B.; Bakken, V.; Adamo, C.; Jaramillo, J.; Gomperts, R.; Stratmann, R. E.; Yazyev, O.; Austin, A. J.; Cammi, R.; Pomelli, C.; Ochterski, J. W.; Ayala, P. Y.; Morokuma, K.; Voth, G. A.; Salvador, P.; Dannenberg, J. J.; Zakrzewski, V. G.; Dapprich, S.; Daniels, A. D.; Strain, M. C.; Farkas, O.; Malick, D. K.; Rabuck, A. D.; Raghavachari, K.; Foresman, J. B.; Ortiz, J. V.; Cui, Q.; Baboul, A. G.; Clifford, S.; Cioslowski, J.; Stefanov, B. B.; Liu, G.; Liashenko, A.; Piskorz, P.; Komaromi, I.; Martin, R. L.; Fox, D. J.; Keith, T.; Al-Laham, M. A.; Peng, C. Y.; Nanayakkara, A.; Challacombe, M.; Gill, P. M. W.; Johnson, B.; Chen, W.; Wong, M. W.; Gonzalez, C.; Pople, J. A. *Gaussian 03 (Revision A.1)*; Gaussian Inc.: Pittsburgh, PA, 2003.

(48) Paschen, D.; Geiger, A. *MOSCITO 3.9;* Department of Physical Chemistry: University of Dortmund, 2000.

(49) Berendsen, H. J. C.; Postma, J. P. M.; van Gusteren, W. F.; Di Nola, A.; Haak, J. R. *J. Chem. Phys.* **1984**, *81*, 3684.

(50) Darden, T.; York, D.; Pedersen, L. *J. Chem. Phys.* **1993**, *98*, 10089.

(51) Essmann, U.; Perera, L.; Berkowitz, M.; Darden, A.; Lee, H.; Pedersen, L. J. *Chem. Phys.* **1995**, *103*, 8577.

(52) Ryckaert, J. P.; Ciccotti, G.; Berendsen, H. J. C. *J. Comput. Phys.* **1977**, *55*, 3336.

(53) Jorgensen, W.; McDonald, N. *J. Mol. Struct.* **1998**, *424*, 145.

(54) McDonald, N.; Jorgensen, W. *J. Phys. Chem. B* **1998**, *102*, 8049.

(55) Thomas, L.; Christakis, T.; Jorgensen, W. *J. Phys. Chem. B* **2006**, *110*, 21198.

(56) Jorgensen, W.; Madura, J.; Swenson, C. *J. Am. Chem. Soc.* **1984**, *106*, 6638.

(57) Jorgensen, W. *J. Phys. Chem.* **1996**, *90*, 6397.

CT700113H